



**HAL**  
open science

# Targeting Mucin Protein Enables Rapid and Efficient Ovarian Cancer Cell Capture: Role of Nanoparticle Properties in Efficient Capture and Culture

Nathan Feely, Anita Wdowicz, Anne Chevalier, Ying Wang, Peng Li, Fanny Rollo, Gil U Lee

## ► To cite this version:

Nathan Feely, Anita Wdowicz, Anne Chevalier, Ying Wang, Peng Li, et al.. Targeting Mucin Protein Enables Rapid and Efficient Ovarian Cancer Cell Capture: Role of Nanoparticle Properties in Efficient Capture and Culture. *Small*, 2023, 19 (18), 10.1002/smll.202207154 . hal-04285688

**HAL Id: hal-04285688**

**<https://hal.science/hal-04285688v1>**

Submitted on 14 Nov 2023

**HAL** is a multi-disciplinary open access archive for the deposit and dissemination of scientific research documents, whether they are published or not. The documents may come from teaching and research institutions in France or abroad, or from public or private research centers.

L'archive ouverte pluridisciplinaire **HAL**, est destinée au dépôt et à la diffusion de documents scientifiques de niveau recherche, publiés ou non, émanant des établissements d'enseignement et de recherche français ou étrangers, des laboratoires publics ou privés.



Distributed under a Creative Commons Attribution 4.0 International License

# Targeting Mucin Protein Enables Rapid and Efficient Ovarian Cancer Cell Capture: Role of Nanoparticle Properties in Efficient Capture and Culture

Nathan Feely, Anita Wdowicz, Anne Chevalier, Ying Wang, Peng Li, Fanny Rollo, and Gil U. Lee\*

The development of specific and sensitive immunomagnetic cell separation nanotechnologies is central to enhancing the diagnostic relevance of circulating tumor cells (CTCs) and improving cancer patient outcomes. The limited number of specific biomarkers used to enrich a phenotypically diverse set of CTCs from liquid biopsies has limited CTC yields and purity. The ultra-high molecular weight mucin, mucin16 (MUC16) is shown to physically shield key membrane proteins responsible for activating immune responses against ovarian cancer cells and may interfere with the binding of magnetic nanoparticles to popular immunomagnetic cell capture antigens. MUC16 is expressed in ≈90% of ovarian cancers and is almost universal in High Grade Serous Epithelial Ovarian Cancer. This work demonstrates that cell bound MUC16 is an effective target for rapid immunomagnetic extraction of expressor cells with near quantitative yield, high purity and viability from serum. The results provide a mechanistic insight into the effects of nanoparticle physical properties and immunomagnetic labeling on the efficiency of immunomagnetic cell isolation. The growth of these cells has also been studied after separation, demonstrating that nanoparticle size impacts cell-particle behavior and growth rate. These results present the successful isolation of “masked” CTCs enabling new strategies for the detection of cancer recurrence and select and monitor chemotherapy.

## 1. Introduction


Epithelial ovarian carcinomas (EOCs) are the fifth leading cause of female cancer mortality worldwide, with an overall 5 year survival rate of 45%.<sup>[1]</sup> Standard treatments for ovarian cancer currently involve surgical removal of the tumor followed by chemotherapy. However, developing resistance to chemotherapeutics during treatment, concluding with recurrence, is common, highlighting the importance of technologies that enable advanced diagnostic methods to monitor cancer progression and patient response to treatment.<sup>[2]</sup> Liquid biopsies are key to enabling these diagnostic methods thanks to their minimally invasive impact on cancer patients and the multitude of cancer biomarkers that may present, ranging from proteins, circulating nucleic acids, extracellular vesicles, and circulating tumor cells.<sup>[3,4]</sup> Circulating cancer cells (CTCs) are cells originating from a tumor that have undergone the epithelial to mesenchymal transition (EMT) and are shed into the bloodstream with the potential for

further metastatic development. The advent of bio-nanotechnologies has enabled the isolation of CTCs from liquid biopsies, resulting in their application as a prognostic indicator for cancer patients.<sup>[5]</sup> More recently, interest in CTCs has evolved beyond prognostic value, to mapping cancer landscapes on an individual basis, facilitating precision approaches to cancer management with potentially high impact outcomes.<sup>[6]</sup> However, unmet challenges remain for the highly sensitive CTC capture necessary for meaningful cancer mapping that enables precision oncology.

Immunomagnetic cell isolation methods have emerged as an enabling technology for the positive enrichment of CTCs from liquid biopsies for downstream quantification (see **Figure 1**). These methods are based on identifying a suitable antigen expressed selectively on the surface of CTCs and capturing expressor cells using antibody (Ab) functionalized superparamagnetic nanoparticles (NPs). Epithelial cell adhesion molecule (EpcAM) is a cell surface protein that characterizes cells of epithelial origin and is a standard target of commercially available

N. Feely, A. Wdowicz, G. U. Lee  
Conway Institute for Biomedical Research and School of Chemistry  
University College Dublin  
61 Adair, Sandymount Ave, Dublin, CO. DUBLIN 00004, Ireland  
E-mail: gil.lee@ucd.ie

A. Chevalier, Y. Wang, P. Li  
Magnostics Ltd  
2 Clifton Lane, Merrion Road, Monkstown, Dublin A94 A306, Ireland  
F. Rollo  
École nationale supérieure des ingénieurs en arts chimiques  
et technologiques  
Toulouse 31030, France

 The ORCID identification number(s) for the author(s) of this article can be found under <https://doi.org/10.1002/smll.202207154>.

© 2023 The Authors. Small published by Wiley-VCH GmbH. This is an open access article under the terms of the Creative Commons Attribution License, which permits use, distribution and reproduction in any medium, provided the original work is properly cited.

DOI: 10.1002/smll.202207154

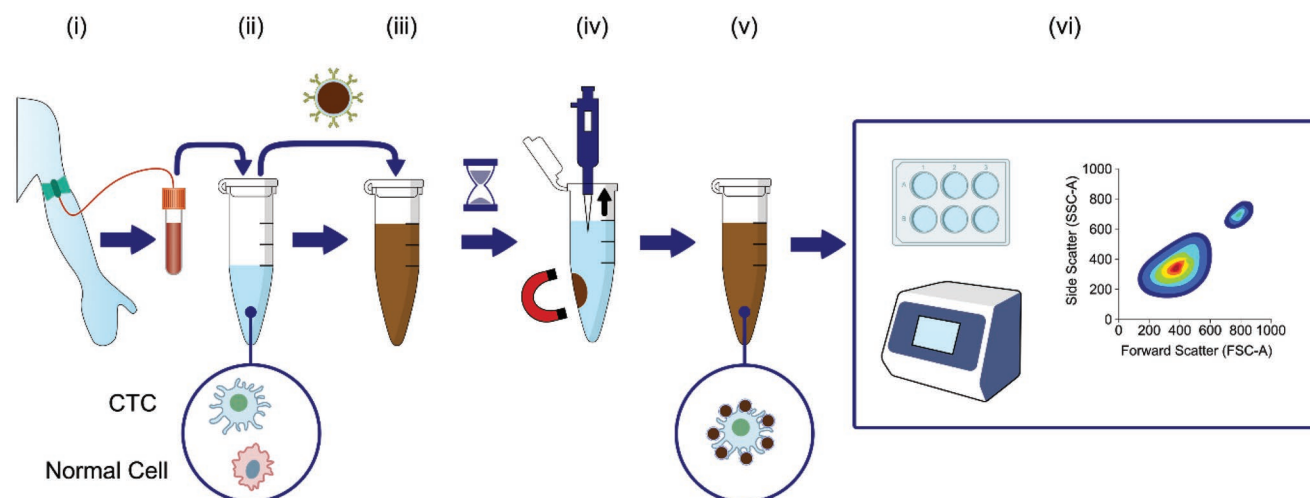


**Figure 1.** Illustration of the CTC isolation workflow from liquid biopsy obtained from cancer patient. i) Blood for the liquid biopsy is drawn from patient. ii) Patient sample containing a low concentration of CTCs in the presence of normal cells is added to reaction tube. iii) Immunomagnetic NPs coated with suitable Ab are added to the patient sample (blood cells may first be separated by centrifugation). NPs bind to CTCs expressing antigen selected for magnetic capture. iv) Following appropriate incubation period, NPs along with labelled cells are captured by addition of magnet. Supernatant containing non-antigen expressor cells is removed from magnetic pellet. v) Magnet is removed and pellet containing labelled CTCs is resuspended in desired buffer. vi) Isolated CTCs can be propagated and/or assessed in-vitro to enable precision cancer treatment for patients.

and U.S. Food and Drug Administration approved CTC enumeration platforms. However, such mono-antigenic platforms do not account for the phenotypic plasticity that is characteristic of cancer cells, especially CTCs, as they up-regulate and down-regulate EpCAM at different stages of the EMT and mesenchymal-epithelial transition (MET) processes resulting in low CTC capture efficiencies, particularly for EOC derived CTCs.<sup>[7–9]</sup> Indeed, the low sensitivity of CTC capture associated with EpCAM has led to the development of immunomagnetic separations with other CTC surface proteins, for example, folic acid receptors,<sup>[10–12]</sup> resulting in EOC CTC capture efficiencies as high as 80%. While this represents a marked improvement, less than quantitative CTC capture could provide an incomplete map of the cancer landscape to determine further treatment options, acting as a barrier to the companion diagnostic utility of CTCs. As such, there is an urgent need to further develop quantitative EOC CTC capture techniques to ensure the potential impacts of precision oncology are realized for ovarian cancer patients.<sup>[6–8]</sup>

Mucin proteins make up mucus, a slippery substance that lubricates and protects the lining of the airways, digestive system, reproductive system, and other organs and tissues. Carbohydrate antigen 125 (CA125) is a peptide sequence that occurs in 11th tandem repeat region in the extracellular domain of the highly glycosylated ultra-high molecular weight ( $\approx 5$  million Da) mucin, MUC16.<sup>[13]</sup> CA125 is overexpressed and shed by ovarian cancer cells resulting in elevated serum CA125 levels detectable in 52% of early-stage and 90% of later-stage ovarian cancer patients. The glycosylated structure of this ultra-high molecular weight mucin is understood to play a key role in immune system evasion with the large size of the mucin acting as a physical barrier preventing natural killer cells binding to key activating cell surface receptors.<sup>[14]</sup> MUC16 has also been observed to interact with several cell adhesion molecules such as mesothelin, e and p-selectin and is recognized as playing a

pro-metastatic role by promoting cell motility and adhesiveness with some studies explicitly highlighting its presence on cancer cells with metastatic potential.<sup>[1,13,15–17]</sup> It has been observed that membrane bound high molecular weight mucins shield CTCs from immune responses, specifically the binding of natural killer cells.

We hypothesize that this shielding mechanism could also interfere with the binding of immunomagnetic NPs to CTCs by shielding membrane protein targets, such as EpCAM and folic acid receptors, located directly at the membrane interface. Given the key role of MUC16 in metastatic progression any potential under-representation of high expressor CTCs from a liquid biopsy could have a significant deleterious impact on clinical recommendations. Therefore, the use of the more accessible MUC16 antigen, CA125 as a target for positive CTC enrichment would be a promising route toward improving the capture efficiency of MUC16 expressor CTCs from liquid biopsies, increasing their clinical relevance in monitoring the response of ovarian cancer patients to treatment. To our knowledge, no studies have examined the application of CA125 as a surface antigen in positive CTC immunomagnetic cell enrichment.

## 2. Results and Discussion

### 2.1. Characterization of Streptavidin (SAv) NPs

Immunomagnetic capture of CTCs was achieved using Ab conjugated superparamagnetic NPs. We studied different cell labeling strategies, such as, direct and in-direct immunomagnetic labeling; using SAv functionalized NPs in combination with biotinylated antibodies selected to label CA125 expressing cell lines. SAv NPs were prepared using different sizes of silica coated iron oxide ( $\text{Fe}_3\text{O}_4$ ) core-shell high magnetization

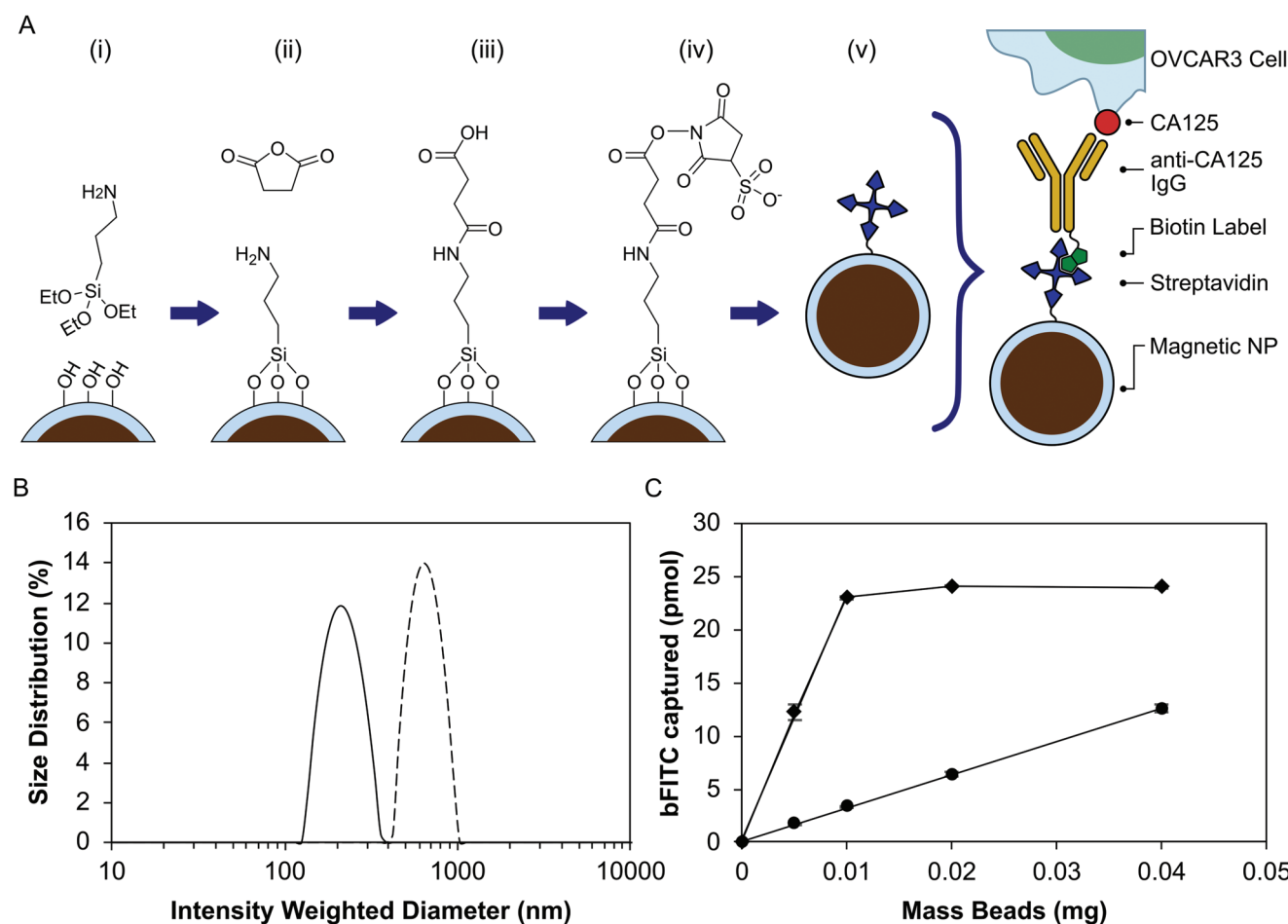
NPs.<sup>[18–21]</sup> These silica coated NPs were amine functionalized by condensation deposition of 3-aminopropyl triethoxysilane from an ethanolic solution followed by conversion of the terminal amine group to a carboxylic acid through a ring opening reaction with succinic anhydride. The immobilization of SAV was achieved through EDC/NHS activation of the surface carboxylic acid groups followed by incubation with SAV (see Figure 2A).<sup>[22,23]</sup> The diameter and monodispersity of the NPs were monitored using DLS, as shown in Figure 2B. The hydrodynamic diameter of the nominal 200 and 800 nm NPs was measured to be 230 nm with a PDI of 8.3 and 730 nm with a PDI of 11%, respectively.

Figure S1, Supporting Information, presents scanning electron micrographs of the SAV 200 and 800 nm NPs. The NPs were observed to have rough surface textures.

The density of immobilized SAV was confirmed using a biotin capture assay developed to quantify the biotin binding capacity of SAV NPs. Increasing masses of SAV NPs were incubated with a known volume of biotin-labeled fluorescein (bFITC) stock

solution before magnetically separating the NPs and measuring the fluorescence loss of the supernatant, the amount of bFITC captured was determined from the percentage fluorescence loss. Figure 2C presents a plot of the calculated bFITC capture as a function of the mass of SAV NPs used to perform the biotin capture. The binding capacity of the SAV NPs can be determined from the slope of the linearly increasing region of the plot. The bFITC captured by 800 nm SAV NPs increased linearly across all masses of NPs tested while the bFITC captured by 200 nm SAV NPs increased rapidly before proceeding to plateau at 25 pmol mg<sup>-1</sup>, a result of capturing all the bFITC added to the assay. Linear regression analyses were performed only on the linear portions of the bFITC capture plots. Binding capacities of 2330 and 320 pmol mg<sup>-1</sup> were measured for 200 and 800 nm NPs, respectively, while a binding capacity of 650–910 pmol mg<sup>-1</sup> was noted for commercially available 2800 nm SAV NPs.

We calculated the biotin binding capacities of spherical NPs with diameters of 200 and 800 nm for a monolayer of SAV,



**Figure 2.** Synthesis and characterization of SAV functionalized superparamagnetic NPs used for immunomagnetic cell separation. A) Overview of synthetic approach toward SAV NPs. i) Preparation of amine functionalized NPs from silica coated NPs described previously via condensation deposition of 3-aminopropyl triethoxysilane from ethanolic solution. ii) Conversion of amine groups to carboxylic acid groups achieved through ring opening reaction with succinic anhydride. iii) EDC/NHS activation of carboxyl functionalized NPs to form NHS activated esters. iv) Immobilization of SAV through incubation with NHS activated NPs to form stable amide bonds between SAV and NPs yielding SAV functionalized NPs. v) Overview of SAV NP binding to CA125(+) cell line. B) DLS size distribution analysis of 200 (solid line) and 800 nm (dashed) SAV NPs. C) Determination of biotin capture capacity of 200 (◆) and 800 nm (●) NPs by measuring capture of biotin-fluorescein (bFITC) conjugate.

that is, results summarized Figure S2, Supporting Information. The binding capacity of the 800 nm NPs was calculated to lie between 312 to 468 pmol mg<sup>-1</sup>, in reasonable agreement with the measured value of 320 pmol mg<sup>-1</sup>. The binding capacity for the 200 nm NPs was calculated to lie between 990–1485 pmol mg<sup>-1</sup>. This range was lower than the measured biotin binding capacity of 2330 pmol mg<sup>-1</sup>. The calculations assume a spherical NP with a smooth surface, an assumption which runs contrary to the SEM analysis of the 200 nm NPs, presented in Figure S1, Supporting Information. We anticipate that the roughness of the 200 nm NPs will produce a higher surface area and streptavidin coverage.

## 2.2. CA125 Expression and Biotinylation in OVCAR3 and A2780 Cells

The selective capture of ovarian cancer cells based on MUC16 expression was investigated using two epithelial ovarian cancer cell lines with different CA125 expression profiles, OVCAR3 (CA125+) and A2780 (CA125-).<sup>[24]</sup> The expression of CA125 on both cell lines was confirmed with a fluorescence immunolabeling experiment where both cell lines were incubated with the anti-CA125 Ab followed by a fluorescently labeled secondary Ab. Fluorescence intensities were monitored using flow cytometry. Figure 3A presents the median fluorescence intensity values of cells following the labeling procedure. OVCAR3 cells were strongly fluorescent for all Ab concentrations tested. The fluorescence intensity increased rapidly with a plateau at Ab concentrations higher than 6 μg mL<sup>-1</sup>, indicating complete labeling of CA125 receptors.

A2780 cells did not yield a fluorescence signal significantly above that of the non-treated negative control indicating the CA125 Ab was not reactive toward this cell line. This result suggests that OVCAR3 cells strongly express CA125 whereas A2780 cells do not, consistent with the known expression of CA125 in both cell lines.<sup>[24]</sup> This demonstrates that the Ab selected for cell labeling discriminates effectively between the cell lines.

Biotinylation of the anti-CA125 Ab was performed to facilitate immunomagnetic labeling of the ovarian cancer cells using SA<sub>v</sub> NPs. The degree of biotinylation was quantified using the FluReporter biotin quantitation kit (see Figure S2, Supporting Information). The biotinylation reaction successfully incorporated biotin labels onto the anti-CA125 Ab with a degree

of labeling of 4.6 ± 0.3 biotins per IgG. Ovarian cancer cells, A2780 cells specifically, have been reported to overexpress a range of vitamin receptors including biotin (vitamin B7) receptors. Indeed, this has been exploited as a mechanism to potentially improve the specificity of cancer treatments through the biotinylation of chemotherapeutic agents such as dendritic polymers loaded with cisplatin.<sup>[25]</sup> In the context of this research, selective biotinylation of OVCAR3 cells through specific antigen interactions between CA125 and the biotinylated Ab is critically important to maximize the specificity of immunomagnetic cell separation. Therefore, the impact of biotinylation on the specificity of IgG binding to both cell lines was examined by labeling CA125 biotinylated cells with fluorescent SA<sub>v</sub>. Figure 3B presents MFI values of cells incubated with increasing concentrations of biotinylated Ab. The OVCAR3 and A2780 cell lines followed a similar trend as was observed for non-biotinylated Ab (see Figure 3A) with high specificity toward the OVCAR3 cell line. The OVCAR3 cells were strongly fluorescent, with maximum fluorescence intensities approximately double those achieved in Figure 3A, a result of using a different fluorescent label. A plateau in the fluorescence intensity occurred, however, the more gradual increase of the binding isotherm in Figure 3B indicates that the biotinylated Ab had a lower binding affinity than the non-biotinylated counterpart. To quantify the Ab binding affinity approximate *K<sub>d</sub>* values were extracted from the binding isotherms. The non-biotinylated and biotinylated antibodies had *K<sub>d</sub>* values of ≈11.0 and 24.3 nM, respectively, indicating that biotinylation impacted the binding affinity of the Ab. This may be explained by biotinylation of amine groups within the Fab region of the Ab, thereby impacting antigen recognition due to the non-specific nature of the sulfo-NHS chemistry used for biotinylation, however, this did not significantly impact the specificity of cell labeling

## 2.3. CA125 Biotinylation and In-Direct Immunomagnetic Separation

The effect of the degree of cellular biotinylation on immunomagnetic cell separation was assessed by incubating OVCAR3 and A2780 cell lines with different concentrations of biotinylated Ab and proceeding to incubate the biotinylated cells with 800 nm SA<sub>v</sub> NPs for immunomagnetic cell capture. Figure 4A presents the percentage cell separation achieved

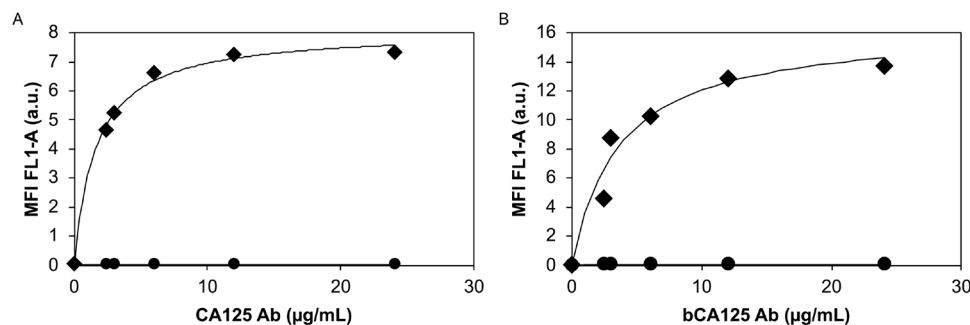


**Figure 3.** Analysis of anti-CA125 Ab binding to OVCAR3 (◆) and A2780 (●) cells analyzed using fluorescence staining and flow cytometry. Median fluorescence intensity values (MFI) are presented. A) Analysis of IgG binding using anti-CA125 Ab with fluorescence labeling using a fluorescent secondary anti-mouse IgG. B) Analysis of biotinylated IgG binding with fluorescence labeling using a fluorescent SA<sub>v</sub> conjugate.



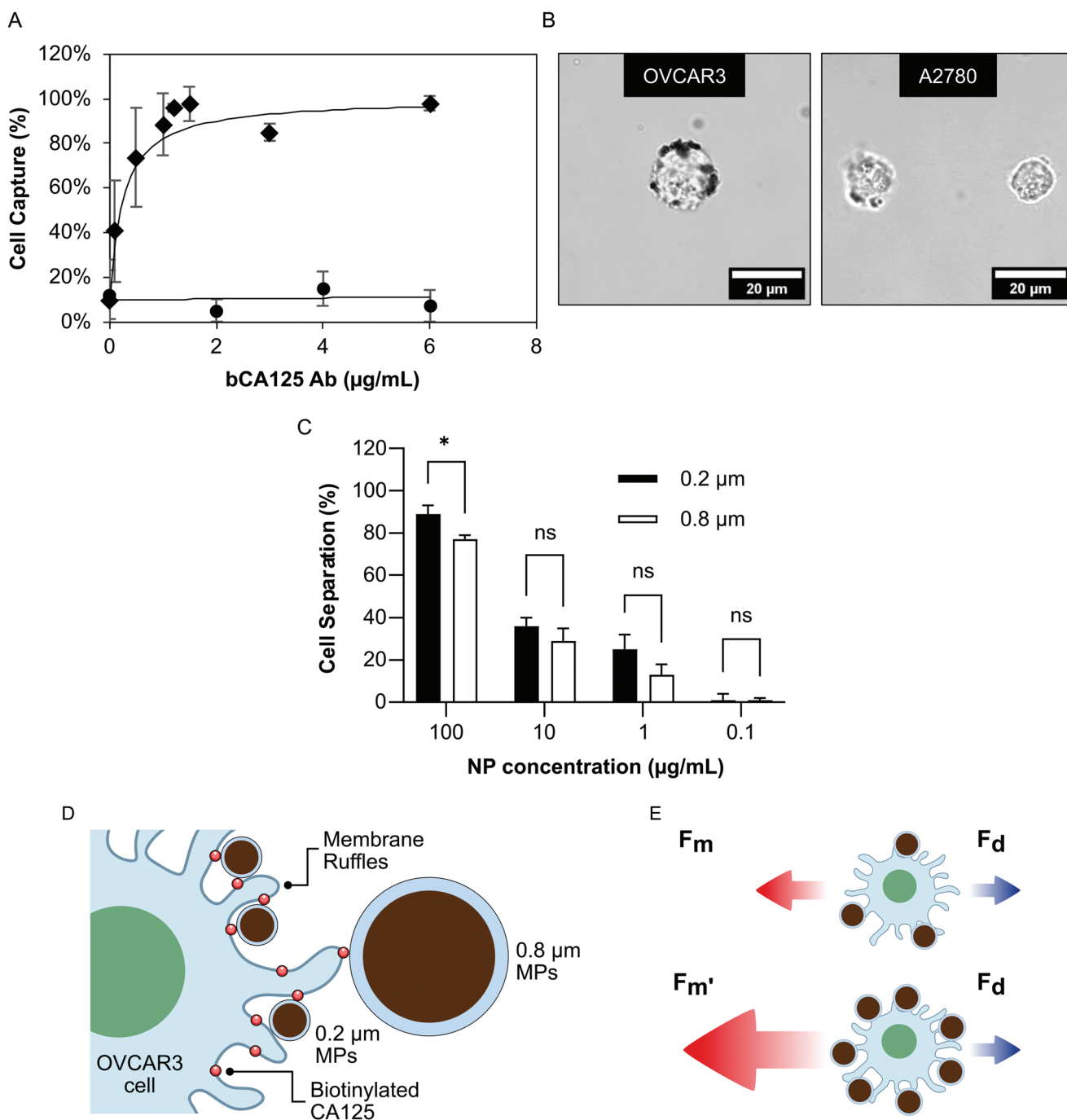


**Figure 4.** Immunomagnetic cell separations performed using SAV NPs. A) Determination of effect degree of cellular biotinylation has on cell capture yields. Separations performed on from samples containing 10 000 cells biotinylated using different concentrations of Ab, in 100  $\mu\text{L}$  following a 30 min incubation with 100  $\mu\text{g mL}^{-1}$  800 nm SAV NPs. B) Brightfield microscope images of anti-CA125 biotinylated cells incubated with 800 nm SAV functionalized NPs. C) Analysis of SAV NP concentration effect on in-direct immunomagnetic capture of OVCAR3 cells labeled using 1  $\mu\text{g mL}^{-1}$  biotinylated Ab solution. Black and white bars represent 200 and 800 nm SAV NPs, respectively. Statistical analysis was performed using a two-way ANOVA test and Bonferroni post-hoc test, where ns denotes not significant and  $*p < 0.05$ . D) Illustration of steric inactivation of large diameter MPs caused by membrane ruffles present on OVCAR3 cells. E) Illustration of effect of low (top) and high (bottom) concentration NPs on number of NPs bound to cells and its effect on total magnetic force ( $F_m$ ) acting on the cell. Higher concentrations of NPs result in larger number of bound NPs resulting in larger magnetic force acting on the cell while the opposing drag force ( $F_d$ ) remains unchanged for a given velocity.

as a function of the Ab concentration used to label the cells. OVCAR3 and A2780 cell lines demonstrated a non-specific capture of 10 and 12%, respectively. The level of A2780 cell separation

did not increase with concentration of biotinylated Ab. OVCAR3 cell separation was strongly dependent on the concentration of biotinylated Ab used to label the cells with the

degree of cell capture increasing rapidly from 0 to  $1 \mu\text{g mL}^{-1}$  before proceeding to plateau at >90% cell separation. Figure 4B presents microscopic imaging performed on the biotinylated cells following incubation with the SA<sub>v</sub> NPs. The NPs were observed to adhere to the surface of the biotinylated OVCAR3 cells and not the A2780 cells. The preferential binding of the NPs and capture of the biotinylated OVCAR3 cells over A2780 cells mirrors the biotinylated Ab binding properties presented in Figure 3B. This indicates that the binding of NPs is mediated by specific SA<sub>v</sub>-biotin interactions. The percentage OVCAR3 cell capture was dependent on the degree of CA125 labeling with a critical degree of labeling achieved at  $1 \mu\text{g mL}^{-1}$  of biotinylated Ab, estimated to represent  $\approx 22\%$  biotinylation of CA125 surface antigens as calculated from the binding isotherm in Figure 3B. Below this concentration the low density of biotinylated CA125 on the cell surface affected the binding affinity of 800 nm SA<sub>v</sub> NPs, reflected in the decreased percentage cell capture.

This low density biotinylated CA125 OVCAR3 cell capture was further investigated by comparing the percentage cell capture achieved using smaller 200 nm SA<sub>v</sub> NPs (see Figure 4C). The OVCAR3 cell capture increased from  $77 \pm 2\%$  to  $89 \pm 4\%$  ( $p < 0.05$ ) with 800 and 200 nm SA<sub>v</sub> NPs, respectively, a 19% improvement in cell capture. This highlights that the size of the NPs can affect the efficiency of binding to the cell surface. Felder et al., revealed the highly uneven surface of OVCAR3 cells and the localization of the CA125 antigen between cell membrane ruffles which were spaced  $\approx 0.5\text{--}1$  nm apart.<sup>[13]</sup> This uneven cellular surface topography highlights the importance of considering the size of NPs used to bind to surface proteins, with smaller NPs encounter less steric resistance enabling them to bind to a greater number of biotinylated antigens located deeper within topographical features of the membrane as illustrated in Figure 4D.

The effect of NP concentration on cell capture efficiency was also investigated. Figure 4C presents the results of cell capture experiments performed on OVCAR3 cells functionalized with  $1 \mu\text{g mL}^{-1}$  of biotinylated Ab and incubated with serial dilutions of 200 and 800 nm SA<sub>v</sub> NPs. The percentage cell capture decreased from  $77 \pm 2\%$  to  $29 \pm 6\%$  on moving from 100 to  $10 \mu\text{g mL}^{-1}$  of 800 nm NPs with a similar trend observed for 200 nm NPs. The magnetic force acting on the labeled cell acts oppositely to the hydrodynamic drag experienced by the cell as its velocity toward the magnet increases. The magnitude of the magnetic force is proportional to the number of NPs bound to the cell.<sup>[12,26]</sup> As the concentration of SA<sub>v</sub> coated NPs decreases, both the rate of NP binding and total number of NPs available is reduced resulting in fewer NPs attached to the cell. This reduces the total magnetic force acting on the cell resulting in overall weaker magnetic forces while the hydrodynamic drag remains largely the same (see Figure 4E). This effect slows the capture of cells toward the magnet and weakens the attractive forces holding cells in place during the fluid flow that occurs when the supernatant is drawn out of the reaction tube. Indeed, higher concentrations of NPs results in more efficient cell capture as more NPs are bound per cell resulting in stronger attractive magnetic forces with the optimal concentration of NPs determined to be  $100 \mu\text{g mL}^{-1}$  for both 200 and 800 nm SA<sub>v</sub> NPs.

#### 2.4. Direct magnetic Cell Separation and Effect of NP Size

Figure 5A presents a comparison of cell capture experiments performed using Ab functionalized NPs against the “in-direct” immunomagnetic procedure described above using  $1 \mu\text{g mL}^{-1}$  of Ab. Ab functionalized NPs were prepared by incubating 200 and 800 nm SA<sub>v</sub> NPs with the biotinylated anti-CA125 Ab. The Ab functionalized NPs were incubated with cells at  $100 \mu\text{g mL}^{-1}$  for 30 min before performing magnetic separation and quantifying the percentage cell capture as before. Improved cell capture yield was noted using this direct capture method with 10 and 28% improvements in percentage cell capture ( $p < 0.01$ ) achieved in comparison to the in-direct method for both 200 and 800 nm NPs, respectively. To ensure high efficiency immunomagnetic cell capture, the total magnetization of the cell must be maximized through binding a large number of NPs. The number of NPs that can bind to a cell is a function of the number of accessible antigen binding sites available (see Figure 4D,E). The number of binding sites available using the in-direct labeling method is further complicated as the antigen must be biotinylated in order for the SA<sub>v</sub> NPs to bind, which is not the case for direct labeling. Therefore, an additional parameter must be included to account for the number of accessible antigen binding sites available for in-direct immunomagnetic cell labeling, the fractional labeling of the antigen. This fractional labeling parameter is not relevant to the direct labeling method resulting in a greater number of available antigen binding sites, which is reflected in the improved cell separation efficiency observed for the direct cell capture experiment.

Figure 5B presents an analysis of the effect of NP size on the incubation time required for efficient cell capture using direct immunomagnetic labeling. OVCAR3 cells were incubated with 200, 800, and 2800 nm Ab NPs at  $100 \mu\text{g mL}^{-1}$  for time points ranging from 1 to 30 min. The diameter of the Ab NPs and efficiency of cell capture were inversely correlated, with 200, 800, and 2800 nm NPs achieving  $90 \pm 8\%$ ,  $77 \pm 12\%$ , and  $41 \pm 9\%$  OVCAR3 cell capture, respectively, following a 1 min incubation. The smaller 200 and 800 nm NPs achieved an equilibrium following 1 min incubation, with no statistically significant improvements in percentage cell capture observed for extended incubation times. By contrast, the percentage cell separation achieved using 2800 nm NPs increased steadily until 20 min of incubation (data not shown) at which point  $79 \pm 11\%$  cell separation was achieved. The level of non-specific A2780 capture was low at  $8 \pm 8\%$ ,  $6 \pm 9\%$ , and  $4 \pm 5\%$  for 200, 800, and 2800 nm NPs, respectively following a 30 min incubation. A strong correlation between NP size and the OVCAR3 capture kinetics was observed with statistically significant improvements in cell separation noted for 200 nm NPs against 2800 nm NPs up to but not including 30 min of incubation ( $p < 0.01$ ).

Indeed, the rate of NP binding to a surface antigen is related to the translational and rotational diffusion coefficient of the NPs as well as the accessibility of different sized NPs for antigens located within the membrane ruffles as discussed in Figure 4D. The theoretical translational ( $D_{\text{Trans}}$ ) and rotational ( $D_{\text{Rot}}$ ) diffusion coefficients are defined by well-known Stokes–Einstein equations, as presented in Figure 5C. The rate of translational particle NP diffusion is determined by solvent temperature and viscosity but is also inversely correlated to the

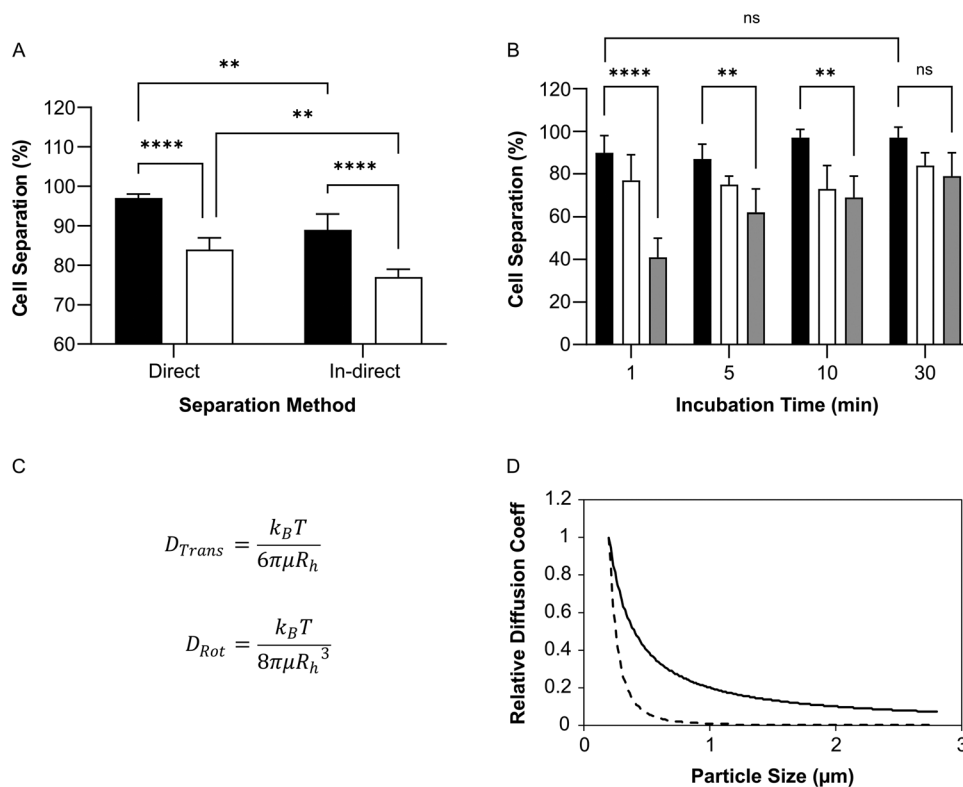


**Figure 5.** Optimization of immunomagnetic cell capture procedure. A) Comparison of direct and in-direct immunomagnetic cell separation experiments using 200 (black) and 800 nm (white) NPs. In-direct immunomagnetic cell separations were performed on samples containing 10 000 cells in 100 μL previously biotinylated using 1 μg mL<sup>-1</sup> biotinylated Ab solution, following a 30 min incubation with 100 μg mL<sup>-1</sup> SA-V NPs. Direct cell separations were performed on samples containing 10 000 cells in 100 μL following a 30 min incubation with 100 μg mL<sup>-1</sup> Ab NPs. B) Analysis of NP incubation time effect on cell separation yield. Cell separations were performed as described for direct immunomagnetic cell separations in (A) with different NP/cell incubation times. Black, white and grey bars represent 200, 800, and 2800 nm Ab NPs, respectively. Statistical analyses were performed using a two-way ANOVA test and Bonferroni post-hoc test, where ns denotes not significant, \*\**p* < 0.01 and \*\*\*\**p* < 0.0001. C) Theoretical Stokes–Einstein translational ( $D_{Trans}$ ) and rotational ( $D_{Rot}$ ) diffusion of a NP of hydrodynamic radius  $R_h$  in a solvent with viscosity ( $\mu$ ) and temperature ( $T$ ). The Boltzmann constant is denoted as ( $k_B$ ). D) Graphical representation of the Stokes–Einstein equations and the effect of NP radius on translational (solid) and rotational (dashed) diffusion coefficients normalized to values for 200 nm NPs.

hydrodynamic radius, while the rotational diffusion coefficient is inversely correlated to the third power of the hydrodynamic radius of the NP. The 800 and 2800 nm NPs have translational diffusion coefficients 4 and 14 times smaller than observed for the 200 nm NPs. The reduced rates of diffusion becoming even more pronounced when considering the rotational diffusion coefficient of the NPs with 800 and 2800 nm NPs yielding 64 and 2744 times smaller rates of rotational diffusion than observed for 200 nm NPs (see Figure 5D). In combination, the reduced rates of translational and rotational diffusion observed for larger MPs severely restricts the mobility and degree of freedom of immobilized antibodies thereby reducing the rate of cell binding for larger diameter MPs. The reduction in the amount of MPs bound to the cells in turn results in weaker magnetic forces cell causing reduced percentage cell capture for short reaction times.

## 2.5. Mixed Cell Separation and Further Propagation

Figure 6A presents a comparison of direct immunomagnetic cell separations performed on mixed cell samples using 200,

800, and 2800 nm NPs. A2780 cells were fluorescently labeled with a membrane soluble fluorescent dye (Vybrant-DiO) to enable identification of each cell population during the separation experiment. OVCAR3 cells were captured with yields of 97 ± 4%, 95 ± 3%, and 87 ± 3% using 200, 800, and 2800 nm NPs, respectively, mirroring similar NP size dependent trends observed for single cell population separations described in Figure 5B with statistically significant improvements in cell capture yields noted for 200 nm NPs in comparison to 2800 nm NPs (*p* < 0.05). The level of non-specific A2780 capture was considerably lower at 17 ± 4%, 16 ± 6%, and 12 ± 6% representing enriched OVCAR3 cell purities of 85%, 86%, and 87% and for 200, 800, and 2800 nm NPs, respectively. No statistically significant comparisons between NP size and non-specific capture of A2780 cells were observed. Figure S4, Supporting Information, presents brightfield and fluorescence microscopy images of the mixed cell sample i) before magnetic separation, ii) the OVCAR3 depleted supernatant, and iii) the OVCAR3 enriched magnetic pellet after magnetic cell capture. The mixed cell sample separation data presented in Figure 6A and Figure S4, Supporting Information, are consistent with the results obtained above for single cell populations and demonstrates



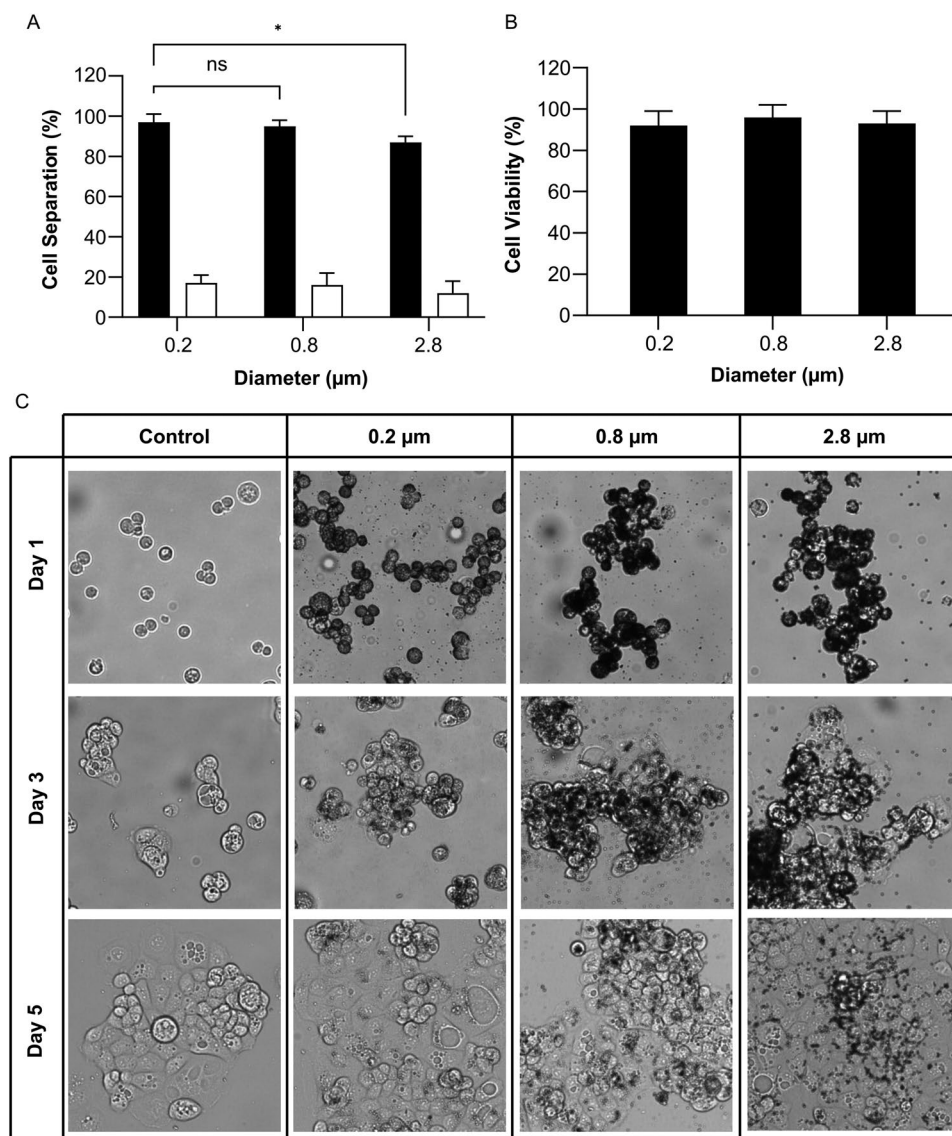


**Figure 6.** Immunomagnetic cell separation performed on a mixed cell population. A) Quantification of cell separation performance from mixed cell samples. Black and white bars represent OVCAR3 and A2780 cells, respectively. Cell separations were performed using direct capture with identical conditions described in Figure 5A on a sample that contained 10 000 OVCAR3 and 10 000 A2780 cells in 100  $\mu\text{L}$ . Statistical analysis was performed using a two-way ANOVA test and Bonferroni post-hoc test, where ns denotes not significant ( $p > 0.05$ ) and  $*p < 0.05$ . B) Quantification of OVCAR3 cell viability following direct immunomagnetic cell separation. Cell viability was assessed by MTS assay to quantify metabolic activity of immunomagnetically captured cells. C) Analysis of cell viability by propagating OVCAR3 cells captured following immunomagnetic cell separation.

that CA125 is a highly effective surface marker for immunomagnetic separation of expressor ovarian cancer cells from non-expressing cells.

The maintenance of cellular viability is critically important to maximize the propagation potential of CTCs following immunomagnetic cell capture through enabling in vitro testing to identify CTC populations with high metastatic potential or developing chemotherapeutic resistance.<sup>[27]</sup> Figure 6B presents an analysis of the viability of OVCAR3 cells immediately following magnetic capture by measuring metabolic activity using the 3-(4,5-dimethylthiazol-2-yl)-5-(3-carboxymethoxyphenyl)-2-(4-sulfophenyl)-2H-tetrazolium (MTS) assay. OVCAR3 cells were captured using Ab NPs at  $100 \mu\text{g mL}^{-1}$  with a 30 min

incubation and the MTS colorimetric response of the captured cells was immediately compared against untreated cells. A high degree of cellular viability was observed for all NPs tested with  $92 \pm 7\%$ ,  $96 \pm 6\%$ , and  $93 \pm 6\%$  recorded for OVCAR3 cells captured with 200, 800, and 2800 nm NPs, respectively. The viability of magnetically captured cells was further investigated by assessing the propagation potential. OVCAR3 cells were resuspended in fresh cell culture medium immediately after magnetic capture and plated in a six well culture plate with the NPs still attached. The cells were cultured over a 5 day period with a medium change after the first 24 h and every 48 h thereafter. Detachment of each NP tested from the cells was observed during the incubation period (see Figure 6C),

however, different rates of detachment were observed for different sizes of NPs. Near complete detachment of 200 nm NPs was noted by the presence of a darkened background caused by a layer of settled NPs following the first 24 h of cell culture (image not presented). Detachment of 800 and 2800 nm NPs occurred more gradually over a 5 day incubation period. The detachment of NPs is consistent with shedding of membrane bound MUC16. However, the different rates of NP detachment observed for 200 nm NPs in comparison to 800 and 2800 nm NPs highlights size dependent variation in cell-NP interactions. Though the origin of this difference is not immediately clear, it may be explained by the smaller surface area of the 200 nm NPs resulting in fewer interactions between NPs and CA125 binding sites.

The morphological appearance of cells immediately following immunomagnetic separation was also noted to change depending on NP size. Cells treated with 200 nm NPs had a similar morphological appearance to the control cell culture, that is, relatively monodisperse, while cells treated with 800 and 2800 nm NPs were present as larger cell clumps. We interpret this to mean the 800 and 2800 nm NPs caused a higher degree of cellular crosslinking in contrast to the behavior observed with 200 nm NPs. In spite of these differences in cellular morphology, all immunomagnetically captured cell lines demonstrated a significant rate of cellular division and cell spreading on the culture dish by day 5 of incubation, indicating cellular propagation potential was preserved following immunomagnetic separation.

### 3. Conclusions

The results presented in this study demonstrate for the first time that MUC16 is an effective target for immunomagnetic capture of expressor CTCs from serum with high capture yield, purity and that the separated cells can be readily cultured. Near quantitative capture yields (>95%) of OVCAR3 cells with greater than 85% purity and 92% viability was observed for 200 and 800 nm SA<sub>v</sub> NPs. We observed rapid rates of OVCAR3 capture for 200 and 800 nm NPs with  $90 \pm 8\%$  and  $77 \pm 12\%$  cell capture, respectively, following a 1 min incubation. This is in contrast with incubation times ranging from 20–120 min reported for similar immunomagnetic capture platforms using other targets such as EpCAM and folic acid receptors.<sup>[10,12,28]</sup> The ultra-high molecular weight of MUC16 has been observed to sterically inactivate NK cells by preventing the binding of key activating receptors, with potential to also inhibit the binding of Ab functionalized NPs to popular immunomagnetic separation targets located closer to cell membrane such as EpCAM and folic acid receptors. Direct targeting of MUC16 antigen CA125 has resulted in enhanced cell-NP interactions improving the efficiency of cell capture.

While a comprehensive study regarding the prevalence of CA125 on real world EOC derived CTCs has not been published, studies have demonstrated that CA125 is present on ovarian cancer CTCs with metastatic potential.<sup>[16]</sup> Indeed, other mucins overexpressed by ovarian cancer cells such as MUC1, have been shown to be effective targets for labeling and detecting EOC derived CTCs in liquid biopsies with fluorescent NPs.<sup>[29]</sup>

MUC16 (CA125), in combination with other CTC markers have potential for increasing CTC capture efficiencies to near-quantitative levels, enabling the representative CTC sampling necessary for meaningful cancer mapping that informs precision oncology.

More broadly, important physicochemical considerations in the design and application of NPs in immunomagnetic cell capture have emerged from this research. We observed that larger 800 and 2800 nm NPs resulted in lower cell capture yields and clumped cellular morphological appearance, whereas 200 nm NPs yielded the highest separation yields and monodisperse morphologies. We attribute these contrasting results to differences in cell-NP interactions with the cell surface, which stem from the cellular topography induced steric effects. This impacted the accessibility of the surface antigens used as the targets for immunomagnetic cell capture for different sizes of NPs, resulting in contrasting morphological appearances and NP shedding behavior during further propagation experiments. Specifically, the smaller NPs used in this study outperformed larger NPs in terms of cell capture yields due to their superior rotational and translational diffusion properties resulting in enhanced cell-NP interactions which maximized the magnetization of CA-125+ OVCAR3 cells.

The facile isolation and culture of CA-125+ ovarian cancer cells using immunomagnetic separation enables a cellular and molecular analysis of the disease. In principle, the magnetic properties of the cells will also allow us to work with individual cells using micromagnetic devices. We anticipate that there are four diagnostic applications for these ovarian CTCs: i) selection of initial chemotherapy; ii) monitoring response to chemotherapy, iii) detecting disease recurrence, and iv) distinguishing malignant from benign pelvic masses. These cells may also be useful in monitoring clinical trials of novel therapeutics.

### 4. Experimental Section

**Materials:** Anti-CA125 mouse monoclonal Ab (GTx21107) was purchased from Genetex (USA). Zeba spin desalting columns 40 K MWCO, EZ-Link sulfo-NHS-LC-biotin, FluorReporter biotin quantitation assay kit, RPMI Medium 1640 with GlutaMAX, penicillin-streptomycin, qualified FBS, L-Glutamine, 2005% Trypsin-EDTA, streptavidin Alexa Fluor 488 conjugate, goat anti-mouse Alexa Fluor 488 conjugate, Dynabeads M-280 streptavidin, Vybrant DiO cell-labeling solution were purchased from Thermo Scientific (UK). Amicon Ultra 10 K MWCO centrifugal filter unit, sodium azide, bovine serum albumin protease free essentially globulin free, insulin from bovine pancreas, phosphate buffered saline tablets were purchased from Merck (UK). T25 polystyrene cell culture flasks were purchased from Greiner. 200 and 800 nm streptavidin functionalized Aurosphere were kindly gifted by Magnostics Ltd (Ireland). OVCAR3 (ATCC HTB161) and A2780 (ECACC Cat No. 93 112 519) cells were kindly gifted by Systems Biology Ireland.

**Biotinylation of CA125 Ab:** CA125 Ab (200 µg) was buffer exchanged into borate buffer (50 mM, pH 8.5) using desalting columns and adjusted to a final volume of ≈170 µL. EZ-link sulfo-NHS LC Biotin (0.5 mg) was dissolved in ice-cold milli-Q water (500 µL). 30 µL of this solution was immediately added to the CA125 Ab solution. The reaction was vortexed and continued at 4 °C for 1 h. Excess biotin reagent was removed by passing the reaction mixture through a desalting column followed by concentration of the biotinylated Ab with a 10K MWCO spin filter. The volume of the concentrated Ab was adjusted to 1 mg mL<sup>-1</sup> using PBS with 0.01% sodium azide and stored at 4 °C until use. The

degree of biotinylation was quantified using the fluorescence biotin quantitation kit as per manufacturer's guidelines.

**Cell Culture of A2780 and OVCAR3 Ovarian Cancer Cell Lines:** A2780 cells were cultured in T25 flasks in RPMI 1640 (with Glutamax) growth medium supplemented with 10% FBS and 1% penicillin/streptomycin at 37 °C in a humidified 5% CO<sub>2</sub> atmosphere. Medium changes were performed every 2–3 days. OVCAR3 cells were cultured in T25 flasks in high glucose RPMI 1640 growth medium, supplemented with 20% FBS, 2 mM L-glutamine, 10 µg mL<sup>-1</sup> bovine insulin and 1% penicillin/streptomycin at 37 °C in a humidified 5% CO<sub>2</sub> atmosphere. Medium changes were performed every 3–4 days. A2780 and OVCAR3 cells were trypsinized for 5 and 8 min, respectively before pelleting and resuspending in PBS with 1% BSA for cell separation assays.

**Fluorescent Immunolabeling of CA125 on Cells:** 10 000 cells in 20 µL of PBS with 1% BSA were treated with 20 µL of serially diluted primary Ab solutions for 30 min at 4 °C. The cells were washed three times using PBS 1% BSA before incubating in 40 µL of a 1:400 dilution of Alexa-488 labeled anti mouse secondary Ab (or Alexa-488 SAv if testing binding of biotinylated primary Ab) solution for 30 min at 4 °C. The fluorescently labeled cells were washed three times and suspended in 100 µL of PBS 1% BSA solution for measurement by flow cytometry.

**In-Direct Magnetic Cell Separation and NP Titration:** 1 00 000 cells were labeled with 100 µL of biotinylated Ab serial dilutions for 30 min at 4 °C in PBS with 1% BSA. SAv NPs were washed three times using PBS with 1% BSA and stocks of 100, 10, 1, or 0.1 µg mL<sup>-1</sup> were prepared. 10 000 biotinylated cells were incubated with 100 µL of the SAv NP dilutions at 4 °C with occasional mixing by inverting the tube for 30 min. Separation was achieved by placing the sample next to a magnet for 3–5 min to allow a pellet to form. The percentage cell separation was determined by the remaining cell count in the supernatant measured using flow cytometry (BD Accuri C6) referenced against the cell count of the cell stock solution. Two-way ANOVA with Bonferroni post-hoc test was performed using GraphPad Prism to make comparisons between samples. Comparisons were determined to be statistically significant where  $p < 0.05$ .

**Preparation of Ab Functionalized NPs:** SAv NPs (200 µg) were washed three times with PBS and incubated in 50 µL PBS solution with 10 µg of biotinylated Ab at r.t. for 1 h on rotating wheel. The NPs were magnetically separated and washed three times using PBS with 1% BSA. The anti-CA125 NPs were kept at 4 °C and used within 24 h.

**Direct Magnetic Cell Separation:** 10 000 cells were incubated with 100 µL of anti-CA125 functionalized NPs at 100 µg mL<sup>-1</sup> at 4 °C with occasional mixing by inverting the tube for 30 min. Separation was achieved by placing the sample next to a magnet for 3–5 min to allow a pellet to form. The percentage cell separation was determined by the remaining cell count in the supernatant measured using flow cytometry referenced against the cell count of the control cell solution.

**Direct Magnetic Mixed Cell Separation:** Direct SPM mixed cell separations were performed as described for direct SPM cell separations. The cell stock contained a 1:1 mixture of OVCAR3 and fluorescently labeled A2780 cells to enable easy identification of cell populations during flow cytometry analysis. The A2780 cells were fluorescently labeled using Vybrant DiO cell labeling solution. In brief, 5 µL of Vybrant DiO cell labeling solution was added to  $1 \times 10^6$  cells in 1 mL of PBS with 1% BSA. The solution was mixed and incubated at 37 °C for 30 min. Excess dye was removed by washing the cells thrice with PBS with 1% BSA. A stock cell solution containing  $1 \times 10^6$  cells mL<sup>-1</sup> each of OVCAR3 and fluorescently labeled A2780 cells was prepared for immunomagnetic cell separation assays. The cell stock was maintained at 4 °C in darkness and used within 4 h to prevent loss of fluorescence. A2780 cells were identified as a fluorescent cell population distinct from the non-fluorescent OVCAR3 cells and gated as such for flow cytometry analysis.

**MTS Cell Viability Assay:** Cell viability following immunomagnetic separation was assessed using an MTS assay which quantifies the metabolic activity of cells via a colorimetric response. 20 000 OVCAR3 cells were incubated with 200 µL of Ab NPs at 100 µg mL<sup>-1</sup> in PBS 1% BSA for 30 min. The cells were immunomagnetically captured for 5 min and redispersed into solution by gentle pipetting before spinning cells

and NPs out of solution at 400 RCF for 5 min. The supernatant was discarded before resuspending cells and NPs in 200 µL of cell medium. The cell solutions were added to a 96-well plate with 20 µL of MTS assay reagent and mixed by gentle shaking. Samples containing untreated cells and magnetic NPs only were treated in a similar manner in tandem with the immunomagnetically captured samples as controls. The plate was incubated at 37 °C for 4 h and the OD490 of each well was measured on a plate reader. Cell viability was calculated as the percentage OD490 of treated cells in comparison to the untreated cells.

**Cell Culture Following Magnetic Cell Separation:** 1 00 000 OVCAR3 cells in 100 µL of PBS with 1% BSA were incubated with 900 µL of anti-CA125 functionalized NPs at 4 °C with occasional mixing by inverting the tube for 30 min. Separation was achieved by placing the sample next to a magnet for 3–5 min to allow a pellet to form. The supernatant was discarded, and the pellet was washed using OVCAR3 cell culture medium. The pellet was resuspended in complete cell culture medium and placed into a 6 well culture dish. The cells were imaged and incubated at 37 °C in a humidified 5% CO<sub>2</sub> atmosphere. A medium change was performed after the first 24 h and every 48–72 h thereafter as necessary. Microscope images of the cells were captured every 24 h.

## Supporting Information

Supporting Information is available from the Wiley Online Library or from the author.

## Acknowledgements

The authors would like to thank Prof. Donald Brennan of the UCD School of Medicine for providing the OVCAR3 and A2780 ovarian cancer cell lines used in this research. This work was supported by Science Foundation Ireland (15/IA/3127).

Open access funding provided by IReL.

## Conflict of Interest

The authors declare no conflict of interest.

## Author Contributions

N.F. methodology, validation, analysis, investigation, visualization, and writing. A.W. methodology, analysis, and investigation. R.F. investigation. A.C., Y.W., and P.L. validation and resources. G.L. concept, writing, supervision.

## Data Availability Statement

The data that support the findings of this study are available in the supplementary material of this article.

## Keywords

CA125, cell capture, cell nanoparticle interactions, cell targeting, circulating tumor cells, diagnostics, MUC16, superparamagnetic nanoparticles

Received: November 17, 2022

Revised: January 18, 2023

Published online: February 11, 2023

- [1] P. Charkhchi, C. Cybulski, J. Gronwald, F. O. Wong, S. A. Narod, M. R. Akbari, *Cancers (Basel)* **2020**, *12*, 3730.
- [2] R. Pokhriyal, R. Hariprasad, L. Kumar, G. Hariprasad, *Biomarker Cancer* **2019**, *11*, 1179299X1986081.
- [3] M. Ignatiadis, G. W. Sledge, S. S. Jeffrey, *Nat. Rev. Clin. Oncol.* **2021**, *18*, 297.
- [4] F. Li, H. Xu, Y. Zhao, *TrAC, Trends Anal. Chem.* **2021**, *145*, 116453.
- [5] W. J. Allard, J. Matera, M. C. Miller, M. Repollet, M. C. Connelly, C. Rao, A. G. J. Tibbe, J. W. Uhr, L. W. M. M. Terstappen, *Clin. Cancer Res.* **2004**, *10*, 6897.
- [6] M. Labib, S. O. Kelley, *Mol. Oncol.* **2021**, *15*, 1622.
- [7] J. F. Liu, D. Kindelberger, C. Doyle, A. Lowe, W. T. Barry, U. A. Matulonis, *Gynecol. Oncol.* **2013**, *131*, 352.
- [8] Z. Eslami-S, L. E. Cortés-Hernández, C. Alix-Panabières, *Cells* **2020**, *9*, 1836.
- [9] J. Yang, S. Cheng, N. Zhang, Y. Jin, Y. Wang, *Biochim. Biophys. Acta, Rev. Cancer* **2022**, *1877*, 188660.
- [10] Y. Pan, Z. Wang, J. Ma, T. Zhou, Z. Wu, P. Ding, N. Sun, L. Liu, R. Pei, W. Zhu, *Biosensors* **2022**, *12*, 184.
- [11] C. Daglioglu, *J. Pharm. Sci.* **2018**, *107*, 934.
- [12] L. Nie, F. Li, X. Huang, Z. P. Aguilar, Y. A. Wang, Y. Xiong, F. Fu, H. Xu, *ACS Appl. Mater. Interfaces* **2018**, *10*, 14055.
- [13] M. Felder, A. Kapur, J. Gonzalez-Bosquet, S. Horibata, J. Heintz, R. Albrecht, L. Fass, J. Kaur, K. Hu, H. Shojaei, *Mol. Cancer* **2014**, *13*, 129.
- [14] J. A. A. Gubbels, M. Felder, S. Horibata, J. A. Belisle, A. Kapur, H. Holden, S. Petrie, M. Migneault, C. Rancourt, J. P. Connor, *Mol. Cancer* **2010**, *9*, 11.
- [15] P. Bottoni, R. Scatena, *Adv. Exp. Med. Biol.* **2015**, *867*, 229.
- [16] W. He, H. Wang, L. C. Hartmann, J. X. Cheng, P. S. Low, *Proc. Natl. Acad. Sci. USA* **2007**, *104*, 11760.
- [17] H. Zhang, Y. Yang, Y. Wang, X. Gao, W. Wang, H. Liu, H. He, Y. Liang, K. Pan, H. Wu, *J. Ovarian Res* **2015**, *8*,.
- [18] C. Holohan, S. Hanrahan, N. Feely, P. Li, J. O'Connell, C. Moss, M. Carr, O. Tagit, G. U. Lee, *Nanoscale* **2021**, *13*, 15659.
- [19] C. Holohan, N. Feely, P. Li, G. Curran, G. U. Lee, *Nanoscale* **2022**, *14*, 12153.
- [20] J. J. O'Mahony, M. Platt, D. Kilinc, G. Lee, *Langmuir* **2013**, *29*, 2546.
- [21] W. Stober, A. Fink, *J. Colloid Interface Sci.* **1968**, *26*, 62.
- [22] Y. An, M. Chen, Q. Xue, W. Liu, *J. Colloid Interface Sci.* **2007**, *311*, 507.
- [23] P. D. Quevedo, T. Behnke, U. Resch-Genger, *Anal. Bioanal. Chem.* **2016**, *408*, 4133.
- [24] E. Yue, G. Yang, Y. Yao, G. Wang, A. Mohanty, F. Fan, L. Zhao, Y. Zhang, T. Mirzapozova, T. C. Walser, *Cancers (Basel)* **2021**, *13*, 4265.
- [25] V. K. Yellepeddi, A. Kumar, D. M. Maher, S. C. Chauhan, K. K. Vangara, S. Palakurthi, *Anticancer Res.* **2011**, *31*, 897.
- [26] H. Huang, C. Ruan, J. Lin, M. Li, L. M. Cooney, W. F. Oliver, Y. Li, A. Wang, *Trans. ASABE* **2011**, *54*, 1015.
- [27] A. Agarwal, M. Balic, D. El-Ashry, R. J. Cote, *Cancer J.* **2018**, *24*, 70.
- [28] Z. Wang, N. Sun, H. Liu, C. Chen, P. Ding, X. Yue, H. Zou, C. Xing, R. Pei, *ACS Appl. Mater. Interfaces* **2019**, *11*, 39586.
- [29] J. H. Kim, H. H. Chung, M. S. Jeong, M. R. Song, K. W. Kang, J. S. Kim, *Int. J. Nanomed.* **2013**, *8*, 2247.